



Evaluating tropospheric nitrogen dioxide in UKCA using OMI satellite retrievals over South and East Asia

Alok K. Pandey^{1,2}, David S. Stevenson¹, Alcide Zhao¹, Richard J. Pope^{3,4}, Ryan Hossaini⁵, Krishan Kumar⁶, Martyn P. Chipperfield^{3,4}

5 ¹School of GeoSciences, University of Edinburgh, Edinburgh, EH9 3FF, UK

²Department of Environmental Sciences, Deshbandhu College, University of Delhi, New Delhi, India

³School of Earth and Environment, University of Leeds, Leeds, LS2 9JT, UK

⁴National Centre for Earth Observation, University of Leeds, Leeds, L22 9JT, UK

⁵Lancaster Environment Centre, Lancaster University, Lancaster, UK

10 ⁶School of Environmental Sciences, Jawaharlal Nehru University, New Delhi, India

Correspondence to: Alok K. Pandey (Alok.Pandey@ed.ac.uk) and David S. Stevenson (David.S.Stevenson@ed.ac.uk)

Abstract. We compare tropospheric column nitrogen dioxide (NO₂) in the United Kingdom Chemistry and Aerosol (UKCA) model version 11.0 with satellite measurements from NASA's Earth Observing System (EOS) Aura satellite Ozone Monitoring Instrument (OMI) to investigate the seasonality and trends of tropospheric NO₂ over South and East Asia (S/E Asia). UKCA is the atmospheric composition component of the UK Earth System Model (UKESM). UKCA was run with nudged meteorology, producing hourly output over S/E Asia for 2005–2015. OMI averaging kernels have been applied to the model hourly data sampled at Aura's local overpass time of 13:45±15 to allow consistent model-data comparison. Background UKCA and OMI tropospheric column NO₂ typically ranges between 0–2 × 10¹⁵ molecules/cm². Diurnal cycles and vertical profiles of the tropospheric NO₂ column in UKCA show that the daily minimum tropospheric column NO₂ occurs around the satellite overpass time. UKCA captures the seasonality but overestimates NO₂, by a factor of ~2.5, especially during winter over Eastern China and North India, at times and locations with high aerosol loadings. Heterogeneous chemistry is represented in the version of UKCA used here as uptake of N₂O₅ on internally generated sulfate aerosol. However, aerosol surface area may be underestimated in polluted locations, contributing to overestimation of NO₂. In addition, the model may underestimate emissions of volatile organic compounds and associated peroxy acetyl (PAN) formation, leading to insufficient long-range transport of oxidised nitrogen, also contributing to overestimation of NO₂ over polluted regions and underestimation over remote regions. Quantifying and understanding discrepancies in modelled NO₂ warrant further investigation as they propagate into modelling of multiple environmental issues.

1 Introduction

30 Nitrogen oxides are key gases in atmospheric chemistry, and models need to simulate them adequately in order to faithfully represent many important environmental processes. Nitrogen dioxide (NO₂) plays a central role in the atmospheric nitrogen cycle (Fowler et al., 2013) and is a precursor of the greenhouse gas (GHG) tropospheric ozone (Bucsela et al., 2008; von



Schneidmesser et al., 2015) and nitrate aerosols (Liu et al., 2016), hence contributing to climate change (Lelieveld et al., 2015). It also affects the oxidising capacity of the global atmosphere, and therefore influences other GHGs such as methane (Naik et al., 2013; Voulgarakis et al., 2013). Large concentrations of NO₂ can also increase the risk of acute and chronic
35 respiratory diseases (Brunekreef et al., 2009). Deposition of NO₂ and other species containing reactive nitrogen can lead to the eutrophication of ecosystems and loss of biodiversity (Stevens et al., 2004; Erisman et al., 2013).

About 95% of anthropogenic emissions of oxides of nitrogen (NO_x: the sum of NO₂, and nitric oxide, NO) are in the form of NO. In the sunlit troposphere, NO reacts with ozone (O₃) to produce NO₂, which photolyzes to return NO and O₃, rapidly forming a photochemical equilibrium. NO₂ is mainly removed by dry deposition and via oxidation to nitric acid, which readily
40 deposits. Another sink, in darkness, is heterogeneous uptake of dinitrogen pentoxide (N₂O₅) on the surface of aerosols (Dentener and Crutzen, 1993). The relatively short (few hours) lifetime of NO₂ (e.g., Beirle et al., 2008) leads to strong spatial and temporal variations in its atmospheric abundance. The oxidation products of volatile organic compounds (VOCs) react with NO₂ to form peroxy acetyl nitrates (PANs), key constituents of photochemical smog. Photochemical smog is a brownish-grey haze which not only reduces visibility in the atmosphere but is also a health hazard (Sher, 1998; Beirle et al., 2003; Mallik
45 and Lal, 2014). PANs are stable at low temperatures typical of the upper troposphere, but thermally unstable in the lower troposphere; they facilitate long-range transport of NO₂ from NO_x source regions to remote sites (Fiore et al., 2018).

Atmospheric NO_x originates principally from vehicular exhaust, industrial boilers and electric utilities (David and Nair, 2011). Rising energy demand, urbanization, traffic and industrialization have resulted in significant increases in NO_x emissions (Mijling et al., 2013). About 58% of current total global NO_x emissions come from the fossil fuel combustion, followed by
50 23% from natural emissions and 19% from agriculture and biofuel use (Lelieveld et al., 2015). NO_x emissions have been falling in North America and Europe from 2005 onwards, whereas in China they peaked around 2011 and started decreasing after 2012 (Cooper et al., 2022). In other world regions, including South Asia, NO_x emissions are increasing (Krotkov et al., 2015, Shah et al., 2020, Singh et al., 2023). This study focusses on S/E Asia, home of nearly 50% of the Earth's population.

Emissions can be estimated from 'bottom-up' methods using activity data and emission factors (Madrazo et al., 2018). Satellite
55 measurements provide an independent 'top-down' approach for the determination of emissions using tropospheric column NO₂ (Beirle et al., 2003; Boersma et al., 2011) and inverse models. In the 1990s, the Global Ozone Monitoring Experiment (GOME) showed NO₂ pollution hotspots around the world (Leue et al., 2001). Since 2002, retrievals from the Scanning Imaging Spectrometer for Atmospheric Cartography (SCIAMACHY) have mapped NO₂ pollution at a finer spatial resolution (30 x 60 km²), with global coverage every six days, allowing the detection of trends in NO₂. The launch of the Ozone
60 Monitoring Instrument (OMI) in 2004 (Levelt et al., 2006) started providing even higher spatial resolution information (13 x 24 km²) of trace gases including tropospheric NO₂ (Liu et al., 2016) with daily global coverage (Boersma et al., 2008). Spectrometric observations from satellite show steady upward trends of tropospheric NO₂ in East China up to 2011 (Shah et al., 2020) and India up to 2015 (Krotkov et al., 2015, Singh et al., 2023). Fan et al. (2021) and Cooper et al. (2022) report decreases in column NO₂ over China since 2012, whereas an increase of 12.5% to 29.6% is reported over India from 2005 to
65 2019 (Singh et al., 2023).



Coupled chemistry-climate models (CCMs) help us to understand the complex links between atmospheric composition, in particular GHGs and short-lived climate pollutants, such as NO₂, and climate. The UK Chemistry and Aerosol (UKCA) model, the atmospheric composition component of the UK Earth System Model (UKESM), is employed in this study. The model is nudged towards reanalysis meteorology, in order to represent physical processes such as transport and mixing as realistically as possible. We evaluate modelled NO₂ from UKCA using the spatial and seasonal distributions of OMI NO₂ over South and East Asia (0-50°N and 55-145°E). Because of the high reactivity and short atmospheric lifetime of NO₂, and its anthropogenic sources, its near-surface concentration has a distinct diurnal signature, as well as a dynamically varying vertical profile. OMI takes column NO₂ measurements at a particular time of day (local time 13:45±15 at the Equator); the vertical profile of NO₂ at the time of measurement strongly influences the column amount. This is because OMI measures radiation absorption at specific ultra-violet/visible (UV/vis) wavelengths, sampling air (and hence NO₂) along the ray path from the Sun, via the atmosphere, to the satellite; this ray path depends upon the atmospheric albedo (i.e., cloud amount and height) at the time of measurement. An averaging kernel (AK) is required to translate the vertical profile to a column amount; the AK is a weighting profile that depends upon environmental conditions (e.g., cloud properties) at the time of measurement. The OMI column NO₂ depends upon the AK and the NO₂ vertical profile. Model evaluation therefore requires careful temporal sampling and application of the AK, so that the model is sampled in the same way as OMI samples the atmosphere. To understand the role of boundary layer variability, we investigate how the boundary layer height (BLH) affects UKCA simulated tropospheric column NO₂. In addition to comparing mean values over the time period 2005-2015, we also compare model and satellite trends.

The paper is structured as follows: Section 2 describes the version and experimental set-up of the UKCA model used for simulations and the satellite NO₂ datasets used to evaluate the model. In Section 3, we present model results for diurnal and seasonal variations of the vertical distribution of NO₂ and how they influence the NO₂ column amount, analysing the spatial distribution over South and East Asia and temporal trends over the period 2005-2015, comparing model results with satellite data. We discuss some of the reasons for model-observation discrepancies in Section 4, before drawing conclusions about model performance with respect to representation of NO₂ in Section 5.

90 2 Data and Methods

2.1 UKCA Model

We use the United Kingdom Chemistry and Aerosols (UKCA) model version 11.0 (Archibald et al., 2020). UKCA is an aerosol-chemistry model coupled to the UK Met Office Hadley Centre HadGEM family of climate models. UKCA simulates the atmospheric composition and climate from the surface to the mesosphere (Morgenstern et al., 2009). HadGEM acts as the dynamical core and provides components for large-scale advection, convective transport and boundary layer mixing of chemical and aerosol tracers (O'Connor et al., 2014). The UKCA stratospheric and tropospheric schemes are described and evaluated by Morgenstern et al., (2009), O'Connor et al., (2014) and Archibald et al., (2020). UKCA version 11.0 comprises



the GA7.1 climate model (Walters et al., 2019) with the StratTrop (CheST) chemistry scheme and the GLOMAP-mode aerosol scheme. Aerosol surface area from GLOMAP is used to drive heterogeneous chemistry. The model's horizontal resolution (N96: 1.875° longitude × 1.25° latitude) is much coarser than the satellite data products used. The model is divided into 85 hybrid height levels with the model top at ~85 km. The vertical resolution is finest close to the surface and gradually decreases with height, i.e., layers are concentrated towards the surface, so the boundary layer (BL) is relatively well resolved in the model, with the lowest (surface) level ~18 m thick.

We used a variant of the version 11.0 'release job' (job ID u-bb210; https://www.ukca.ac.uk/wiki/index.php/Release_Job_UM11.0 dated 7th October 2019), adding a meteorological nudging scheme to allow for a more meaningful comparison of satellite data to model output. Nudging (Newtonian relaxation) is a data assimilation technique that adjusts dynamical variables of a free-running general circulation model (GCM) using meteorological reanalysis data to allow a relatively realistic representation of the atmosphere at a given time. For nudging, the European Centre for Medium-range Weather Forecasts (ECMWF) ERA-interim data were used, and the model was run from 2005 to 2015. Monthly varying Coupled Model Intercomparison Project Phase 6 (CMIP 6) anthropogenic and biomass burning emissions of NO_x and other relevant species from AerChemMIP have been used (Collins et al., 2017). No diurnal variations in anthropogenic or biomass burning emissions are applied. Natural emissions are as described by Archibald et al. (2020); in particular, lightning NO_x emissions are interactive and follow the Price and Rind (1992) parameterization, whilst soil NO_x emissions vary monthly but are annually invariant and use the Yienger and Levy (1995) distribution.

2.2 Satellite NO₂ data

The Ozone Monitoring Instrument (OMI) is a nadir-viewing sensor that measures radiation at ultraviolet-visible wavelengths, mounted on NASA's EOS Aura satellite (Boersma et al., 2011; Liu et al., 2016). Aura travels at an altitude of 705 km in a sun-synchronous polar orbit and provides daily global coverage with a daytime local equator crossing time of 13:45±15 minutes (Shah et al., 2019). OMI measures backscattered radiation from Earth's atmosphere and surface over the wavelength range 264 - 504 nm, with a spectral resolution between 0.42 - 0.63 nm and a nadir spatial resolution of 13 × 24 km² (Dobber et al., 2006; Levelt et al., 2006). The instrument consists of a telescopic system using CCD detectors which provide it a 114° field of view corresponding to a large swath of 2600 km at the Earth's surface. OMI retrieves the ozone column and profile, aerosols, SO₂, NO₂ and other trace atmospheric constituents such as HCHO, BrO, and OCIO using the technique of Differential Optical Absorption Spectroscopy (DOAS). OMI tropospheric column NO₂ data utilised here come from the Tropospheric Emission Monitoring Internet Service (TEMIS) product (Boersma et al., 2011) (DOMINO v2.0). The data has been screened to only include data with a cloud fraction of below 0.2 in addition to the good data flags while excluding data with the OMI row anomaly, using the algorithm of Braak (2010). This product includes AK information which have been used for model-satellite comparison.

The AK describes the vertical structure of the atmospheric profile, accounting for the measurement sensitivity at different locations and times (Vijayaraghavan et al., 2008; Boersma et al., 2016). In other words, the AK is a linear representation of



the vertical weighting of information content of retrieval parameters. The AK is specified as a vector, used to provide a measure of the vertical resolution of the estimate (Martin, 2008; Vijayaraghavan et al., 2008). The AKs have been applied to UKCA model NO₂ as shown in Equation 1:

$$y = \mathbf{A} \cdot \mathbf{x} \quad (1)$$

135 where \mathbf{A} is the tropospheric AK, from the OMI product, with vertical values at specific pressures, \mathbf{x} is the model profile (sub-columns in units of molecules/cm²), interpolated to the OMI vertical pressure grid, and y is the modified model tropospheric column (model sub-columns with AKs applied totalled up to the satellite defined tropopause). The AKs of each day have been applied to daily model profiles, which are then averaged to produce monthly means. This modified column is then directly compared to the satellite NO₂ column.

140 In addition to applying the AK, the model data must be sampled at the satellite overpass time. We achieve this by producing hourly model output and matching this to the satellite data. To understand the impacts of sampling at 13:45±15 minutes local time, we compare monthly average NO₂ values (i.e. an average across all times of day) with a monthly average calculated just using values for between 1300-1400 local time.

We focus our analysis on S/E Asia (Figure 1a), dividing this region into six different sub-regions, two politically (India and
145 China) and four geographically (E China, W China, N India, and S India; Figure 1b). We focus on the N India and E China sub-regions for detailed study as these are hot-spots of high population density and high NO₂ emissions (Ramachandran et al., 2013; Sekiya et al., 2018). Figure 1a shows 2015 surface NO emissions; these total around 0.09-0.10 Tg N yr⁻¹ over E China and 0.07-0.08 Tg N yr⁻¹ over N India. Figure 1b shows percentage changes relative to 2005 in the NO surface emissions from 2005 to 2015 (from AerChemMIP, Collins et al., 2017), which show a 40-60% increase in surface NO emissions over this
150 period in India, whereas the increase is relatively smaller (20-40%) in China. The 2005-2015 trends in surface NO emissions integrated over the whole of China and India are shown in Figure 1c. Surface NO emissions from China were 4.8 Tg N yr⁻¹ in 2005, increasing to 6.5 Tg N yr⁻¹ by 2011, followed by a decrease to 5.8 Tg N yr⁻¹ in 2015, as also reported in other studies (Miyazaki et al., 2017, Shah et al., 2020). In contrast, India has shown a consistent upward trend, with NO emissions increasing from 1.8 Tg N yr⁻¹ in 2005 to 2.5 Tg N yr⁻¹ in 2015 (Krotkov et al., 2015).

155 3 Results and discussion

3.1 Seasonal and diurnal variations of the vertical profile of NO₂

Figure 2 shows seasonal and diurnal variation of tropospheric column NO₂ taken directly from the UKCA model (with no vertical weighting) over N India and E China. UKCA tropospheric column NO₂ is generally lower over both regions during the late morning and early afternoon (the satellite overpass time), due to photochemical destruction which peaks around local
160 mid-day, before NO₂ increases in the late afternoon. While NO₂ levels remain high during the evening/night in E China, column values decrease in N India. The diurnal cycle shows the lowest daily range in June-July-August (JJA), varying from ~5-10 × 10¹⁵ molecules/cm² (over N India) and ~9-11 × 10¹⁵ molecules/cm² (E China). By contrast, the December-January-



February (DJF) diurnal cycle shows the largest ranges: $8-17 \times 10^{15}$ molecules/cm² (N India) and $30-55 \times 10^{15}$ molecules/cm² (E China). Seasonal diurnal variations of tropospheric column NO₂ for all sub-regions are shown in Figure S1. It is important
165 to note that the UKCA does not have a diurnal cycle in emissions, so the model doesn't simulate higher NO₂ levels related to real-world processes like late afternoon rush hour. Rather, higher levels of NO₂ in the late afternoon arise solely due to dynamical and photochemical processes.

Figure 3 shows the seasonal variation in vertical profiles of NO₂ over N India and E China, as simulated by the UKCA model. The highest levels of NO₂ are found in the boundary layer, close to sources, and during winter, when the boundary layer is
170 shallowest and when NO₂ loss chemistry proceeds more slowly. Levels of NO₂ above the boundary layer are much lower, and show seasonal maxima in summer at 10 km. NO₂ in the upper troposphere reflects a balance between sources associated with enhanced convection and lightning during the monsoon being partly offset by the higher summer photolysis rates. Equivalent average seasonal vertical profiles (2005-2015) for all regions are shown in Figure S2, whereas Figure S3 show the trends of the vertical profiles from 2005 to 2015 over all regions, which highlights that the vertical extent of NO₂ is relatively less
175 affected by pollution in W China and S India in comparison to E China and N India.

Figure 4 shows the diurnal variation of the NO₂ vertical profiles over the same regions for the four seasons. The solid black line in Figure 4 shows the BLH of the model which is highest during afternoon (~1-2 km). Higher surface NO₂ values occur at night, and the overpass time of OMI is close to the daily minimum values of NO₂ throughout the vertical column, and the maximum BLH. Typically, an increase in the surface NO₂ concentration is observed after sunset, and the modelled BLH
180 rapidly collapses to well below 100 m. Comparative vertical profiles for all regions are shown in Figure S4.

3.2 Model-satellite data comparisons: time sampling and averaging kernel impacts

The importance of time sampling and application of the AK for model-satellite comparison is shown in Figure 5, using monthly mean OMI data averaged over the whole of S/E Asia for 2005, and comparing it with UKCA column NO₂ data generated in several ways: (i) simple monthly mean, with no AK weighting; (ii) time-matched to the satellite overpass time using hourly
185 model data, but with no AK weighting; and (iii) time-matched and modified by the AK weighting. Measurement uncertainty is based on the daily variation over the month.

Figure 5 shows S/E Asia regional mean OMI tropospheric column NO₂ ranges between 1.0 and 2.0×10^{15} molecules/cm² over 2005, with measurement uncertainty $0.5-1.0 \times 10^{15}$ molecules/cm². In comparison, the UKCA simple monthly mean tropospheric column NO₂ values are larger: $2.2-2.5 \times 10^{15}$ molecules/cm² in summer and over 4.0×10^{15} molecules/cm² in
190 winter. Whilst the OMI tropospheric column NO₂ is measured at 13:45 local time (LT), when the NO₂ is typically relatively low (Figures 2 and 4), the modelled simple monthly mean incorporated all time periods. Therefore, the simple monthly mean modelled NO₂ is substantially larger. In contrast, once the diurnal cycle is accounted for (i.e. UKCA is sub-sampled at the satellite overpass time), modelled NO₂ is in much better agreement with OMI, with near zero biases in summer (<1%) but in winter the model still overestimates (by ~80%). When the AKs are applied to the model (in addition to sub-sampling at



195 13:45+15 minutes LT) the summer biases remain near-zero (<1%) and the winter overestimation is reduced (to ~50%) and the model seasonal cycle now sits within the satellite uncertainty range.

Figure 5 clearly demonstrates the importance of accounting for satellite vertical sensitivities and temporal sampling when evaluating model simulations. Applying the correct time sampling is much more important than including the AK effect. In all the subsequent analysis presented here, we only show UKCA NO₂ columns sampled at the overpass time and with the AK
200 applied.

3.3 Seasonal and spatial variations of tropospheric NO₂ column

Figure 6 shows the seasonal distribution of tropospheric NO₂ observed by OMI and simulated by UKCA, averaged between 2005 and 2015 over S/E Asia. The largest tropospheric NO₂ columns can be seen over E. China in DJF from both OMI (>20 × 10¹⁵ molecules/cm²) and UKCA (>30 × 10¹⁵ molecules/cm²). The seasonal minimum (in JJA) tropospheric column values
205 compare well between OMI and UKCA and typically peak around 6-10 × 10¹⁵ molecules/cm². Comparing UKCA and OMI indicates that the model is overestimating tropospheric column NO₂ in the major polluted regions (e.g. E. China, the Indo-Gangetic Plain), especially in DJF. Over E. China the differences range from +50% to +100% in March-April-May (MAM), JJA and September-October-November (SON). In DJF, the model overestimation (over +150%) is more widespread and also covers the pollution outflow regions (e.g. Pacific Ocean). The peak biases in India are also in DJF and are +100% to +150%.
210 In the background, less polluted regions, the model tends to underestimate the observations by up to 100% in all seasons.

Scatter plots of OMI vs. UKCA tropospheric column NO₂ (Figure 7) confirm that UKCA overestimates observations in polluted regions in all seasons. The model generally performs best in JJA, and worst in DJF. UKCA captures the observed spatial variability well with R² values of 0.87, 0.77, 0.89 and 0.88 for MAM, JJA, SON and DJF, respectively. To understand the biases due to the higher values another best fit, after removing the highest 10% of observed values, has been computed and
215 plotted (green line). This shows that the model is performing better over the first 90% of the OMI data, although the fit is not improved in DJF. The main problem with the model appears to be an overestimate of NO₂ column over the most polluted regions, especially in winter.

3.4 Regional OMI and UKCA tropospheric column NO₂ variability

Figure 8 shows time series (2005-2015) of OMI and UKCA simulated tropospheric NO₂ over the whole of India and China, together with over four regions (indicated by the boxes in Figure 1b). OMI tropospheric column NO₂ typically varies between
220 1-2 × 10¹⁵ molecules/cm² over India (Figure 8a) with a relatively small seasonal cycle. Over China tropospheric column NO₂ ranges between 2-4 × 10¹⁵ molecules/cm² (Figure 8b) with more pronounced seasonality. UKCA tropospheric column NO₂ typically ranges between 2-5 × 10¹⁵ molecules/cm² and 2-12 × 10¹⁵ molecules/cm² over India and China, respectively. Seasonality is captured by UKCA but the amplitude is overstated by a factor of 2-3.

Figure 8c and 8d show UKCA and OMI tropospheric column NO₂ over North India and East China where values typically range between 1-2 × 10¹⁵ and 5-20 × 10¹⁵ molecules/cm², respectively. Rapid industrialization, urbanization and increased



230 traffic activity have resulted in a significant increase in the air pollution over E China and N India in the past two-three decades (Ghude et al., 2008a; Kar et al., 2010; Mijling et al., 2013). This can be seen in the OMI data in East China between 2005 and 2011 as tropospheric column NO_2 has increased from approximately 12 to 19×10^{15} molecules/cm². The signal in North India is much smaller. Again, UKCA tropospheric column NO_2 captures the observed seasonality (5 - 12×10^{15} molecules/cm², North India; 4 - 45×10^{15} molecules/cm², East China) but overstates the amplitude. UKCA reproduces the observed trend in East China, but not East India, but overestimates their magnitudes in both cases.

235 OMI and UKCA trends over the relatively clean regions of South India and West China are shown in Figure 8e and 8f, respectively. South India has an OMI lower tropospheric column NO_2 (1 - 2.5×10^{15} molecules/cm²) and UKCA provides a good representation of the observed seasonality and magnitude. UKCA reproduces the observed marginal increase of tropospheric column NO_2 between 2005 and 2011. In West China, the observed tropospheric column NO_2 ranges between 0.5 - 1.5×10^{15} molecules/cm² which UKCA struggles to reproduce in magnitude (~50% lower).

3.5 Trends of NO_2 over the years 2005-2011 and 2011-2015

240 Over China NO_x emission increased by 52% from 2005 to 2011 and thereafter decreased by 21% from 2011 to 2015 (Figure 1c) as reported elsewhere (De Foy et al., 2016; Liu et al., 2017). Therefore, we focus on OMI and UKCA trends over these time periods (Figures 9 and 10). We observed the largest trends in the DJF particularly in the UKCA between 2005 to 2011. The seasonal variations in OMI trends are small between 2005 and 2011, with differences of approximately 0.5×10^{15} molecules/cm²/yr. However, there have been increases in DJF across East China of up to 1.0×10^{15} molecules/cm²/yr, and decreases of up to 0.5×10^{15} molecules/cm²/yr observed over Japan, South Korea and Hong Kong. UKCA shows similar 245 spatial distributions of changes across the majority of the domain, but overstates the magnitudes of decreases over Japan, South Korea, Hong Kong, and increases over East China. There are also substantial model decreases (approximately -1.0×10^{15} molecules/cm²/yr) over East China in SON which are not present in the OMI observations. Between 2011 and 2015, both OMI and UKCA changes show a steady decrease of up to 2.0×10^{15} molecules/cm²/yr over East China in almost all seasons (Figure 10 right panel). There are only small changes in the OMI trends over the India from 2011-2015. Although a decrease of up to 250 0.5×10^{15} molecules/cm²/yr is observed in OMI over North India in DJF (Figure 10 left panel).

Figures 11 and 12 show scatter plots of the seasonal trends between UKCA and OMI over 2005-2011 and 2011-2015 respectively. UKCA overestimates the magnitudes of trends in NO_2 at most locations, with the gradients of best fits (OMI trend over the UKCA trend) in the range 0.15-0.39 for the time period 2005-2011 (Figure 11), but showing a closer correspondence (0.39-0.67) for 2011-2015 (Figure 12), when the NO_2 tropospheric column starts decreasing over China. The 255 overestimation of trends by the model is consistent with the overestimation of NO_2 columns in polluted regions, again with the worst agreement in DJF, and better performance in JJA.



4 Discussion

It is well understood that to usefully compare satellite measurements of column NO₂ with model simulations, the model atmosphere needs to be sampled in the same way that the satellite samples the real atmosphere (e.g., Boersma et al, 2008, 2011, 2016). Sampling UKCA at the OMI overpass time and application of a satellite-derived vertical weighting function (averaging kernel) significantly influence the modelled NO₂ column and make it more comparable to the OMI values (Figure 5), although differences remain, particularly during winter, when UKCA over-estimates NO₂ columns.

The results presented in Figures 2 and 4 illustrate some of the challenges faced by models in accurately simulating column NO₂ values measured by satellite instruments such as OMI, particularly during winter (DJF) and at higher latitudes. Diurnal variations in simulated column NO₂ for N India and E China (Figure 2) show that at the OMI overpass time the column is changing least (it is approximately flat) in JJA, whilst in DJF it is rising towards a late afternoon peak, particularly further north. This means that any errors in the shape of the simulated diurnal cycle of NO₂ will translate into larger errors in column NO₂ in winter and at higher latitudes.

One source of error in the simulated diurnal cycle of NO₂ arises due to the use of diurnally invariant anthropogenic and biomass burning emissions in these UKCA simulations. Boersma et al. (2008) show that using diurnally varying NO_x emissions has significant effects on the diurnal cycle of the simulated NO₂ column, tending to increase it during daylight hours, as this is when more emissions occur. Hence inclusion of diurnally varying emissions would likely exacerbate the model-observation differences seen in this study.

Figures 6 and 7 show that the model is overestimating NO₂ column over the more polluted regions, but underestimating it over the cleaner regions. This may reflect a lack of PAN formation, or equivalent sequestration of NO_x in other reservoir species. PAN is a compound that locks up NO₂ in a reaction with the PA (peroxy acetyl) radical (Fiore et al., 2018). The PA comes from oxidation of certain volatile organic compounds (VOCs). PAN is stable at cold temperatures, but unstable at high temperatures, decomposing back to NO₂ and PA. If PAN formation is too low (e.g., because VOCs are too low), this may cause more NO₂ in source regions, and less transport of NO₂ to remote regions.

Another potential contributing factor to the overestimation of NO₂ in source regions may be underestimation of heterogeneous conversion of N₂O₅ to nitrate aerosol (e.g., Dentener and Crutzen, 1993; Riemer et al., 2003; Chen et al., 2018) in UKCA. These modelling studies have shown that this heterogeneous chemistry tends to reduce NO_x, especially during winter and in polluted regions with high aerosol loads, and it seems likely that the aerosol surface areas simulated by UKCA in these regions are underestimated.

Modelled trends in column NO₂ over S/E Asia are larger than trends seen in the OMI data, particularly during DJF. This is partly explained by the general overestimation of NO₂ columns, especially in polluted areas. Upwards trends in aerosols would tend to enhance heterogeneous loss of oxidised N, so the underestimation of this process in UKCA would lead to an overestimate of NO₂ trends.



5 Conclusions

290 In this work we evaluated tropospheric column NO_2 from the UKCA model using OMI satellite retrievals over S/E Asia. This required sampling the model at the satellite overpass time and application of vertical weighting profiles (averaging kernels) that account for how the satellite retrieval is influenced by the presence of clouds. UKCA can capture the NO_2 seasonality over S/E Asia but overestimates NO_2 column in all seasons, and especially in polluted regions during winter. UKCA overestimates column NO_2 near source regions, but underestimates column NO_2 in remote regions, suggesting it is not converting enough

295 NO_2 into longer-lived reservoir species such as PAN. Overestimations in polluted regions may be due to the UKCA model underestimating heterogeneous conversion of N_2O_5 to nitrate aerosol, which has been shown to quite strongly reduce NO_x levels in the presence of aerosol, which is present at high levels across much of the region. UKCA also overestimates trends in NO_2 column over the region. Underestimation of heterogeneous chemistry may be further contributing to the trend overestimations, as the influence of increases in aerosols over time will be missed.

300 Given the importance of accurate simulation of oxidised N for many processes important to climate, air quality and the wider environment, further investigation of these discrepancies in simulated NO_2 in UKCA are required. In particular, we recommend inclusion of schemes to more comprehensively represent heterogeneous chemistry and diurnal variation of emissions, together with exploration of the VOC emissions and PAN formation mechanisms in the model, to see if their improved representation can lead to improvements in the simulation of column NO_2 .

305

Code and Data Availability: This work used the United Kingdom Chemistry and Aerosol model. The model outputs were pre-processed using netCDF Operator (NCO) and Climate Data Operator (CDO). The analysis was carried out using Python.

Author contributions: AKP and DSS conceptualised and planned the research study. AKP performed the UKCA model simulations with support from DSS. AKP performed the model and satellite data analysis with help of AZ. RJP and MPC

310 helped in the satellite and model data comparison. KK and RH commented on the manuscript. AKP and DSS wrote most of the first draft. All authors helped to shape the paper content by editing prior versions of the paper.

Competing interests: The authors declare that they have no conflict of interest.

Acknowledgements: This work used the ARCHER and ARCHER2 UK National Supercomputing Service (<http://www.archer.ac.uk/> and <https://www.archer2.ac.uk/>, last access: 16 January 2020 and 24 August 2023 respectively).

315 Authors acknowledge ARCHER/ARCHER2 for supercomputing resources. The authors thank the United Kingdom Chemistry and Aerosol team especially Luke Abraham for support in running UKCA model, and Paul Griffiths for helping us to understand the model's heterogeneous chemistry. We are grateful to Mohit Dalvi (Met Office) for providing the model dumps. This work used JASMIN, the UK's collaborative data analysis environment (<http://jasmin.ac.uk>). We acknowledge the NASA Earth Science Division and KNMI for funding the OMI NO_2 development and the archiving of standard and DOMINO

320 products via Tropospheric Emission Monitoring Internet Service (TEMIS - <http://www.temis.nl/index.php>), respectively.



Financial support. AKP acknowledges support from a Commonwealth Rutherford Fellowship (Commonwealth Scholarship Commission grant ID: INRF2017-196) and from the Department of Science and Technology, India, and British Council UK Newton-Bhabha Programme (DST/INSPIRE/NBHF2015/5). DSS acknowledges support from the UKRI Global Challenges Research Fund South Asian Nitrogen Hub (grant NE/S009019/2). Funding for Richard J. Pope and Martyn P. Chipperfield was provided by the UK NERC National Centre for Earth Observation (NCEO).

References

- Archibald, A. T., O'Connor, F. M., Abraham, N. L., Archer-Nicholls, S., Chipperfield, M. P., Dalvi, M., Folberth, G. A., Dennison, F., Dhomse, S. S., Griffiths, P. T., Hardacre, C., Hewitt, A. J., Hill, R. S., Johnson, C. E., Keeble, J., Köhler, M. O., Morgenstern, O., Mulcahy, J. P., Ordóñez, C., Pope, R. J., Rumbold, S. T., Russo, M. R., Savage, N. H., Sellar, A., Stringer, M., Turnock, S. T., Wild, O., and Zeng, G.: Description and evaluation of the UKCA stratosphere–troposphere chemistry scheme (StratTrop v1.0) implemented in UKESM1, *Geosci. Model Dev.*, 13, 1223–1266, <https://doi.org/10.5194/gmd-13-1223-2020>, 2020.
- Beirle, S., Platt, U., Wenig, M. and Wagner, T.: Weekly cycle of NO₂ by GOME measurements: A signature of anthropogenic sources, *Atmos. Chem. Phys.*, 3(6), 2225–2232, doi:10.5194/acp-3-2225-2003, 2003.
- Beirle, S., Boersma, K. F., Platt, U., Lawrence, M. G. and Wagner, T.: Megacity emissions and lifetimes of nitrogen oxides probed from space, *Science* (80-.), 333(6050), 1737–1739, doi:10.1126/science.1207824, 2011.
- Boersma, K. F., Jacob, D. J., Eskes, H. J., Pinder, R. W., Wang, J. and van der A, R. J.: Intercomparison of SCIAMACHY and OMI tropospheric NO₂ columns: Observing the diurnal evolution of chemistry and emissions from space, *J. Geophys. Res. Atmos.*, 113(16), 1–14, doi:10.1029/2007JD008816, 2008.
- Boersma, K. F., Eskes, H. J., Dirksen, R. J., Van Der A, R. J., Veefkind, J. P., Stammes, P., Huijnen, V., Kleipool, Q. L., Sneep, M., Claas, J., Leitão, J., Richter, A., Zhou, Y. and Brunner, D.: An improved tropospheric NO₂ column retrieval algorithm for the Ozone Monitoring Instrument, *Atmos. Meas. Tech.*, 4(9), 1905–1928, doi:10.5194/amt-4-1905-2011, 2011.
- Boersma, K. F., Vinken, G. C. M. and Eskes, H. J.: Representativeness errors in comparing chemistry transport and chemistry climate models with satellite UV-Vis tropospheric column retrievals, *Geosci. Model Dev.*, 9(2), 875–898, doi:10.5194/gmd-9-875-2016, 2016.
- Braak R., Row Anomaly Flagging Rules Lookup Table, KNMI Technical Document TN-OMIE-KNMI-950, KNMI, Netherlands, 2010.
- Brunekreef, B., Hoek, G., Schouten, L., Bausch-goldbohm, S., Fischer, P., Armstrong, B., Hughes, E., Jerrett, M., Brandt, P. Van Den, Beelen, R. and van den Brandt, P.: Effects of long-term exposure to traffic-related air pollution on respiratory and cardiovascular mortality in the Netherlands: the NLCS-AIR study., *Res. Rep. Health. Eff. Inst.*, (139), 5–71; discussion 73–89 [online] Available from: <http://www.ncbi.nlm.nih.gov/pubmed/19554969>, 2009.



- 355 Bucsela, E. J., Perring, A. E., Cohen, R. C., Boersma, K. F., Celarier, E. A., Gleason, J. F., Wenig, M. O., Bertram, T. H.,
Wooldridge, P. J., Dirksen, R. and Veefkind, J. P.: Comparison of tropospheric NO₂ from in situ aircraft measurements with
near-real-time and standard product data from OMI, *J. Geophys. Res. Atmos.*, 113(16), 1–14, doi:10.1029/2007JD008838,
2008.
- Chen, Y., Wolke, R., Ran, L., Birmili, W., Spindler, G., Schröder, W., Su, H., Cheng, Y., Tegen, I., and Wiedensohler, A.: A
parameterization of the heterogeneous hydrolysis of N₂O₅ for mass-based aerosol models: improvement of particulate nitrate
prediction, *Atmos. Chem. Phys.*, 18, 673–689, <https://doi.org/10.5194/acp-18-673-2018>, 2018.
- 360 Collins, J. W., Lamarque, J. F., Schulz, M., Boucher, O., Eyring, V., Hegglin, I. M., Maycock, A., Myhre, G., Prather, M.,
Shindell, D. and Smith, J. S.: AerChemMIP: Quantifying the effects of chemistry and aerosols in CMIP6, *Geosci. Model Dev.*,
10(2), 585–607, doi:10.5194/gmd-10-585-2017, 2017.
- Cooper, M. J., Martin, R. V., Hammer, M. S., Levelt, P. F., Veefkind, P., Lamsal, L. N., Krotkov, N. A., Brook, J. R. and
McLinden, C. A.: Global fine-scale changes in ambient NO₂ during COVID-19 lockdowns, *Nature*, 601(7893), 380–387,
doi:10.1038/s41586-021-04229-0, 2022.
- 365 David, L. M. and Nair, P. R.: Diurnal and seasonal variability of surface ozone and NO_x at a tropical coastal site: Association
with mesoscale and synoptic meteorological conditions, *J. Geophys. Res.*, 116(D10), D10303, doi:10.1029/2010JD015076,
2011.
- Dentener, F. J., and Crutzen, P. J.: Reaction of N₂O₅ on tropospheric aerosols: Impact on the global distributions of NO_x, O₃,
and OH, *J. Geophys. Res.*, 98(D4), 7149–7163, doi:10.1029/92JD02979, 1993.
- 370 Dobber, M. R., Dirksen, R. J., Levelt, P. F., Van Den Oord, G. H. J., Voors, R. H. M., Kleipool, Q., Jaross, G., Kowalewski,
M., Hilsenrath, E., Leppelmeier, G. W., De Vries, J., Dierssen, W. and Rozemeijer, N. C.: Ozone monitoring instrument
calibration, *IEEE Trans. Geosci. Remote Sens.*, 44(5), 1209–1238, doi:10.1109/TGRS.2006.869987, 2006.
- Erismann, J. W., Galloway, J. N., Seitzinger, S., Bleeker, A., Dise, N. B., Roxana Petrescu, A. M., Leach, A. M. and de Vries,
W.: Consequences of human modification of the global nitrogen cycle, *Philos. Trans. R. Soc. B Biol. Sci.*, 368(1621),
375 doi:10.1098/rstb.2013.0116, 2013.
- Fan, C., Li, Z., Li, Y., Dong, J., Van Der A, R. and De Leeuw, G.: Variability of NO₂ concentrations over China and effect on
air quality derived from satellite and ground-based observations, *Atmos. Chem. Phys.*, 21(10), 7723–7748, doi:10.5194/acp-
21-7723-2021, 2021.
- 380 Fiore, A. M., Fischer, E. V., Milly, G. P., Pandey Deolal, S., Wild, O., Jaffe, D. A., Stachelin, J., Clifton, O. E., Bergmann,
D., Collins, W., Dentener, F., Doherty, R. M., Duncan, B. N., Fischer, B., Gilge, S., Hess, P. G., Horowitz, L. W., Lupu, A.,
MacKenzie, I. A., Park, R., Ries, L., Sanderson, M. G., Schultz, M. G., Shindell, D. T., Steinbacher, M., Stevenson, D. S.,
Szopa, S., Zellweger, C. and Zeng, G.: Peroxy acetyl nitrate (PAN) measurements at northern midlatitude mountain sites in
April: A constraint on continental source-receptor relationships, *Atmos. Chem. Phys.*, 18(20), 15345–15361, doi:10.5194/acp-
18-15345-2018, 2018.



- 385 Fowler, D., Coyle, M., Skiba, U., Sutton, M. A., Cape, J. N., Reis, S., Sheppard, L. J., Jenkins, A., Grizzetti, B., Galloway, J. N., Vitousek, P., Leach, A., Bouwman, A. F., Butterbach-Bahl, K., Dentener, F., Stevenson, D., Amann, M. and Voss, M.: The global nitrogen cycle in the Twentyfirst century, *Philos. Trans. R. Soc. B Biol. Sci.*, 368(1621), doi:10.1098/rstb.2013.0164, 2013.
- De Foy, B., Lu, Z. and Streets, D. G.: Satellite NO₂ retrievals suggest China has exceeded its NO_x reduction goals from the
390 twelfth Five-Year Plan, *Sci. Rep.*, 6(December 2013), 1–9, doi:10.1038/srep35912, 2016.
- Ghude, S. D., Fadnavis, S., Beig, G., Polade, S. D. and van der A, R. J.: Detection of surface emission hot spots, trends, and seasonal cycle from satellite-retrieved NO₂ over India, *J. Geophys. Res. Atmos.*, 113(20), 1–13, doi:10.1029/2007JD009615, 2008a.
- Ghude, S. D., Fadnavis, S., Beig, G., Polade, S. D. and van der A, R. J.: Detection of surface emission hot spots, trends, and
395 seasonal cycle from satellite-retrieved NO₂ over India, *J. Geophys. Res.*, 113(D20), D20305, doi:10.1029/2007JD009615, 2008b.
- Kar, J., Deeter, M. N., Fishman, J., Liu, Z., Omar, A., Creilson, J. K., Trepte, C. R., Vaughan, M. A. and Winker, D. M.: Wintertime pollution over the Eastern Indo-Gangetic Plains as observed from MOPITT, CALIPSO and tropospheric ozone residual data, *Atmos. Chem. Phys.*, 10(24), 12273–12283, doi:10.5194/acp-10-12273-2010, 2010.
- 400 Krotkov, N. a., McLinden, C. a., Li, C., Lamsal, L. N., Celarier, E. a., Marchenko, S. V., Swartz, W. H., Bucsela, E. J., Joiner, J., Duncan, B. N., Boersma, K. F., Veefkind, J. P., Levelt, P. F., Fioletov, V. E., Dickerson, R. R., He, H., Lu, Z. and Streets, D. G.: Aura OMI observations of regional SO₂ and NO₂ pollution changes from 2005 to 2014, *Atmos. Chem. Phys. Discuss.*, 15(19), 26555–26607, doi:10.5194/acpd-15-26555-2015, 2015.
- Lelieveld, J., Beirle, S., Hörmann, C., Stenchikov, G. and Wagner, T.: Abrupt recent trend changes in atmospheric nitrogen
405 dioxide over the Middle East, *Sci. Adv.*, 1(7), 1–6, doi:10.1126/sciadv.1500498, 2015.
- Leue, C., Wenig, M., Wagner, T., Klimm, O., Platt, U. and Jahne, and B.: Quantitative analysis of emissions from Global Ozone Monitoring Experiment satellite image sequences, *J. Geophys. Res.*, 106(D6), 5493–5505, 2001.
- Levelt, P. F., Van Den Oord, G. H. J., Dobber, M. R., Mälkki, A., Visser, H., De Vries, J., Stammes, P., Lundell, J. O. V and Saari, H.: The ozone monitoring instrument, *IEEE Trans. Geosci. Remote Sens.*, 44(5), 1093–1100,
410 doi:10.1109/TGRS.2006.872333, 2006.
- Liu, F., Beirle, S., Zhang, Q., Dörner, S., He, K. and Wagner, T.: NO_x lifetimes and emissions of cities and power plants in polluted background estimated by satellite observations, *Atmos. Chem. Phys.*, 16(8), 5283–5298, doi:10.5194/acp-16-5283-2016, 2016.
- Liu, F., Beirle, S., Zhang, Q., van der A, R. J., Zheng, B., Tong, D. and He, K.:
415 NO₂ emission trends over Chinese cities estimated from OMI observations during 2005 to 2015, *Atmos. Chem. Phys. Discuss.*, (2), 1–21, doi:10.5194/acp-2017-369, 2017.



- Madrazo, J., Clappier, A., Belalcazar, L. C., Cuesta, O., Contreras, H., & Golay, F.: Screening differences between a local inventory and the Emissions Database for Global Atmospheric Research (EDGAR). *Science of the Total Environment*, 631, 934-941, 2018.
- 420 Mallik, C. and Lal, S.: Seasonal characteristics of SO₂, NO₂, and CO emissions in and around the Indo-Gangetic Plain, *Environ. Monit. Assess.*, 186(2), 1295–1310, doi:10.1007/s10661-013-3458-y, 2014.
- Martin, R. V.: Satellite remote sensing of surface air quality, *Atmos. Environ.*, 42(34), 7823–7843, doi:10.1016/j.atmosenv.2008.07.018, 2008.
- Mijling, B., Van Der A, R. J. and Zhang, Q.: Regional nitrogen oxides emission trends in East Asia observed from space, 425 *Atmos. Chem. Phys.*, 13(23), 12003–12012, doi:10.5194/acp-13-12003-2013, 2013.
- Miyazaki, K., Eskes, H., Sudo, K., Folkert Boersma, K., Bowman, K. and Kanaya, Y.: Decadal changes in global surface NO_x emissions from multi-constituent satellite data assimilation, *Atmos. Chem. Phys.*, 17(2), 807–837, doi:10.5194/acp-17-807-2017, 2017.
- Morgenstern, O., Braesicke, P., O'Connor, F. M., Bushell, a. C., Johnson, C. E., Osprey, S. M. and Pyle, J. a.: Evaluation of 430 the new UKCA climate-composition model – Part 1: The stratosphere, *Geosci. Model Dev.*, 2, 43–57, doi:10.5194/gmd-2-43-2009, 2009.
- Naik, V., Voulgarakis, A., Fiore, A. M., Horowitz, L. W., Lamarque, J. F., Lin, M., Prather, M. J., Young, P. J., Bergmann, D., Cameron-Smith, P. J., Cionni, I., Collins, W. J., Dalsøren, S. B., Doherty, R., Eyring, V., Faluvegi, G., Folberth, G. A., Josse, B., Lee, Y. H., MacKenzie, I. A., Nagashima, T., Van Noije, T. P. C., Plummer, D. A., Righi, M., Rumbold, S. T., Skeie, 435 R., Shindell, D. T., Stevenson, D. S., Strode, S., Sudo, K., Szopa, S. and Zeng, G.: Preindustrial to present-day changes in tropospheric hydroxyl radical and methane lifetime from the Atmospheric Chemistry and Climate Model Intercomparison Project (ACCMIP), *Atmos. Chem. Phys.*, 13(10), 5277–5298, doi:10.5194/acp-13-5277-2013, 2013.
- O'Connor, F. M., Johnson, C. E., Morgenstern, O., Abraham, N. L., Braesicke, P., Dalvi, M., Folberth, G. a., Sanderson, M. G., Telford, P. J., Voulgarakis, a., Young, P. J., Zeng, G., Collins, W. J. and Pyle, J. a.: Evaluation of the new UKCA climate- 440 composition model-Part 2: The troposphere, *Geosci. Model Dev.*, 7(1), 41–91, doi:10.5194/gmd-7-41-2014, 2014.
- Ramachandran, A., Pallipad, J., Sharma, S. a. and Jain, N. K.: Recent trends in tropospheric NO₂ over India observed by SCIAMACHY: Identification of hot spots, *Atmos. Pollut. Res.*, 4(4), 354–361, doi:10.5094/APR.2013.040, 2013.
- Riemer, N., Vogel, H., Vogel, B., Schell, B., Ackermann, I., Kessler, C., and Hass, H.: Impact of the heterogeneous hydrolysis of N₂O₅ on chemistry and nitrate aerosol formation in the lower troposphere under photosmog conditions, *J. Geophys. Res.*, 445 108, 4144, doi:10.1029/2002JD002436, 2003.
- von Schneidemesser, E., Monks, P. S., Allan, J. D., Bruhwiler, L., Forster, P., Fowler, D., Lauer, A., Morgan, W. T., Paasonen, P., Righi, M., Sindelarova, K. and Sutton, M. A.: Chemistry and the Linkages between Air Quality and Climate Change, *Chem. Rev.*, 115(10), 3856–3897, doi:10.1021/acs.chemrev.5b00089, 2015.
- Sekiya, T., Miyazaki, K., Ogochi, K., Sudo, K. and Takigawa, M.: Global high-resolution simulations of tropospheric nitrogen 450 dioxide using CHASER V4.0, *Geosci. Model Dev.*, 11(3), 959–988, doi:10.5194/gmd-11-959-2018, 2018.



- Shah, V., Jacob, D. J., Li, K., Silvern, R. F., Zhai, S., Liu, M., Lin, J. and Zhang, Q.: Effect of changing NO_x lifetime on the seasonality and long-term trends of satellite-observed tropospheric NO_2 columns over China, *Atmos. Chem. Phys. Discuss.*, (2), 1–23, doi:10.5194/acp-2019-670, 2019.
- 455 Shah, V., J. Jacob, D., Li, K., Silvern, R., Zhai, S., Liu, M., Lin, J. and Zhang, Q.: Effect of changing NO_x lifetime on the seasonality and long-term trends of satellite-observed tropospheric NO_2 columns over China, *Atmos. Chem. Phys.*, 20(3), 1483–1495, doi:10.5194/acp-20-1483-2020, 2020.
- Sher, E.: *Environmental Aspects of Air Pollution*, Woodhead Publishing Limited., 1998.
- Singh, N., Dey, S., & Knibbs, L. D. (2023). Spatio-temporal patterns of tropospheric NO_2 over India during 2005–2019. *Atmospheric Pollution Research*, 14(3). <https://doi.org/10.1016/j.apr.2023.101692>
- 460 Stevens, C. J., Dise, N. B., Mountford, J. O. and J, G. D.: Impact of Nitrogen Deposition Grasslands, *Science* (80-.), 303(March), 1876–1879, 2004.
- T Archibald, A., M O’Connor, F., Luke Abraham, N., Archer-Nicholls, S., P Chipperfield, M., Dalvi, M., A Folberth, G., Dennison, F., S Dhomse, S., T Griffiths, P., Hardacre, C., J Hewitt, A., S Hill, R., E Johnson, C., Keeble, J., O Köhler, M., Morgenstern, O., P Mulcahy, J., Ordóñez, C., J Pope, R., T Rumbold, S., R Russo, M., H Savage, N., Sellar, A., Stringer, M., 465 T Turnock, S., Wild, O. and Zeng, G.: Description and evaluation of the UKCA stratosphere-troposphere chemistry scheme (StratTrop v1.0) implemented in UKESM1, *Geosci. Model Dev.*, 13(3), 1223–1266, doi:10.5194/gmd-13-1223-2020, 2020.
- Vijayaraghavan, K., Snell, H. E. and Seigneur, C.: Practical aspects of using satellite data in air quality modeling, *Environ. Sci. Technol.*, 42(22), 8187–8192, doi:10.1021/es7031339, 2008.
- 470 Voulgarakis, A., Naik, V., Lamarque, J. F., Shindell, D. T., Young, P. J., Prather, M. J., Wild, O., Field, R. D., Bergmann, D., Cameron-Smith, P., Cionni, I., Collins, W. J., Dalsøren, S. B., Doherty, R. M., Eyring, V., Faluvegi, G., Folberth, G. A., Horowitz, L. W., Josse, B., MacKenzie, I. A., Nagashima, T., Plummer, D. A., Righi, M., Rumbold, S. T., Stevenson, D. S., Strode, S. A., Sudo, K., Szopa, S. and Zeng, G.: Analysis of present day and future OH and methane lifetime in the ACCMIP simulations, *Atmos. Chem. Phys.*, 13(5), 2563–2587, doi:10.5194/acp-13-2563-2013, 2013.
- 475 Walters, D., Baran, A. J., Boutle, I., Brooks, M., Earnshaw, P., Edwards, J., Furtado, K., Hill, P., Lock, A., Manners, J., Morcrette, C., Mulcahy, J., Sanchez, C., Smith, C., Stratton, R., Tennant, W., Tomassini, L., Van Weverberg, K., Vosper, S., Willett, M., Browse, J., Bushell, A., Carslaw, K., Dalvi, M., Essery, R., Gedney, N., Hardiman, S., Johnson, B., Johnson, C., Jones, A., Jones, C., Mann, G., Milton, S., Rumbold, H., Sellar, A., Ujiie, M., Whitall, M., Williams, K. and Zerroukat, M.: The Met Office Unified Model Global Atmosphere 7.0/7.1 and JULES Global Land 7.0 configurations, *Geosci. Model Dev.*, 480 12(5), 1909–1963, doi:10.5194/gmd-12-1909-2019, 2019.



485

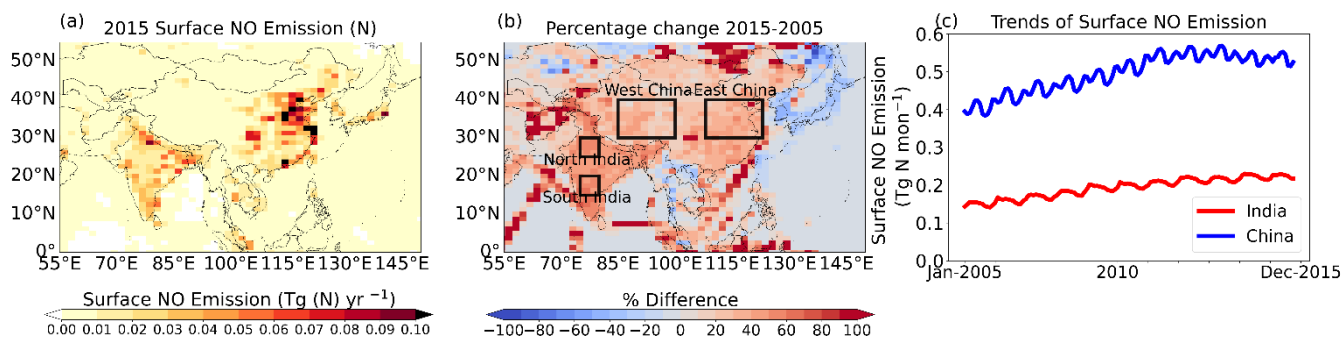


Figure 1 (a) Surface nitrogen oxide (NO) emission over S/E Asia (Tg N yr⁻¹) in 2015; (b) Percentage change in the NO surface emissions from 2005 to 2015; (c) trends of NO surface emissions (Tg N month⁻¹) from 2005 to 2015 over India and China. Boxes shown in (b) indicate regions referred to in the text.



490

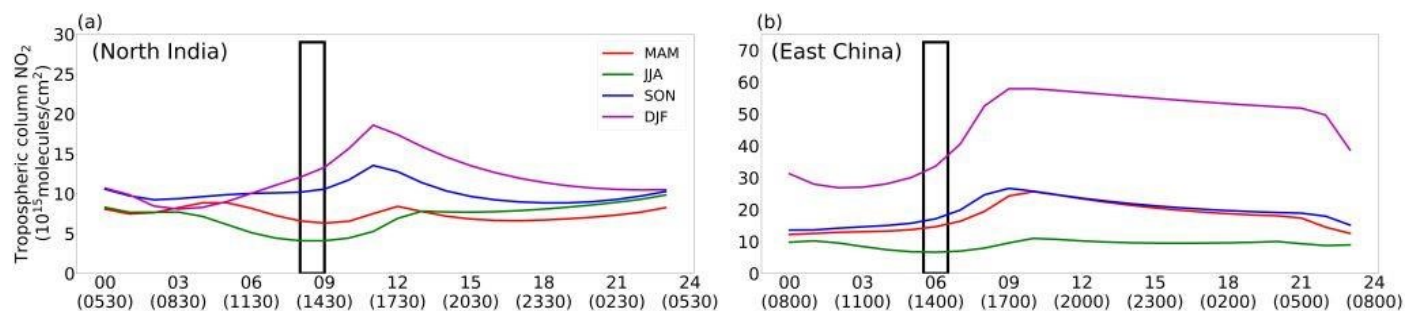


Figure 2 Diurnal cycles of tropospheric column NO₂ (10¹⁵ molecules/cm²) simulated by UKCA over (a) North India and (b) East China for the four seasons (averaged over 2005-2015). The time axis shows the time in UTC and, in brackets, the local time. The box indicates the OMI overpass time.

495

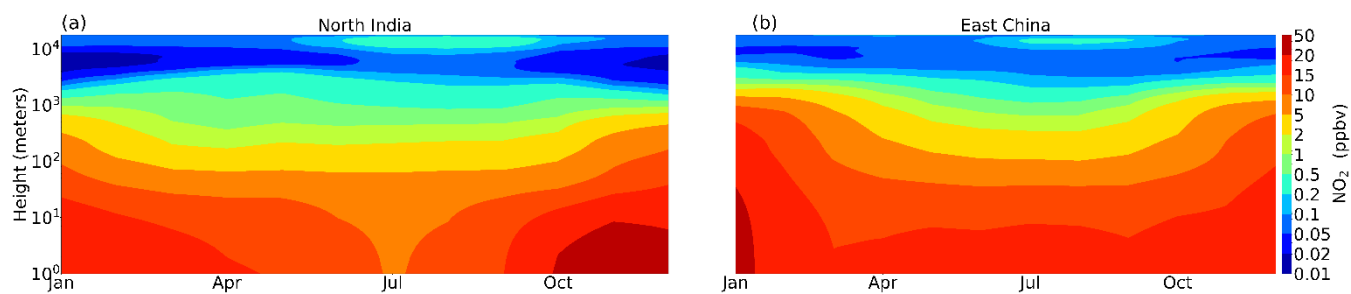
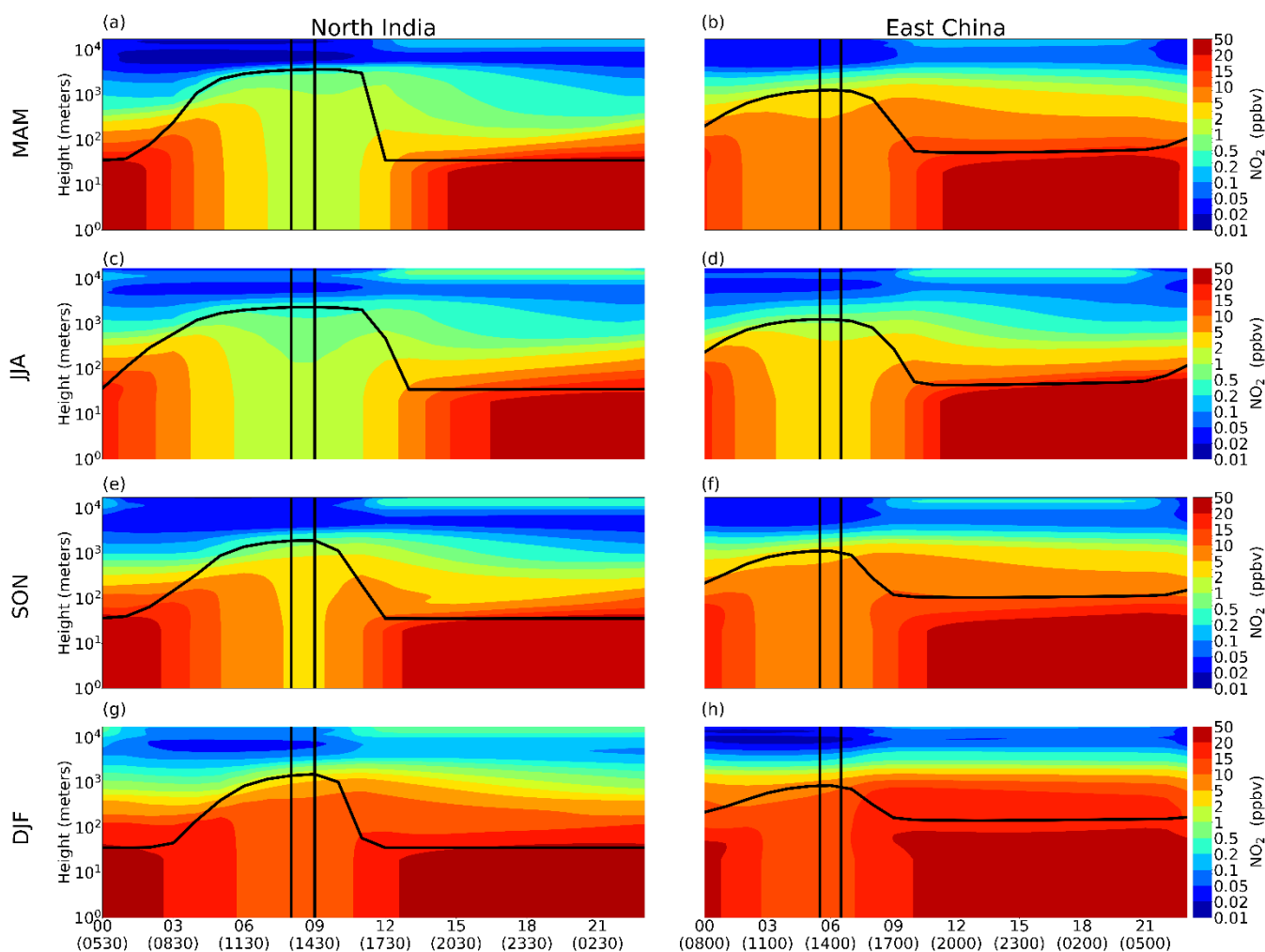
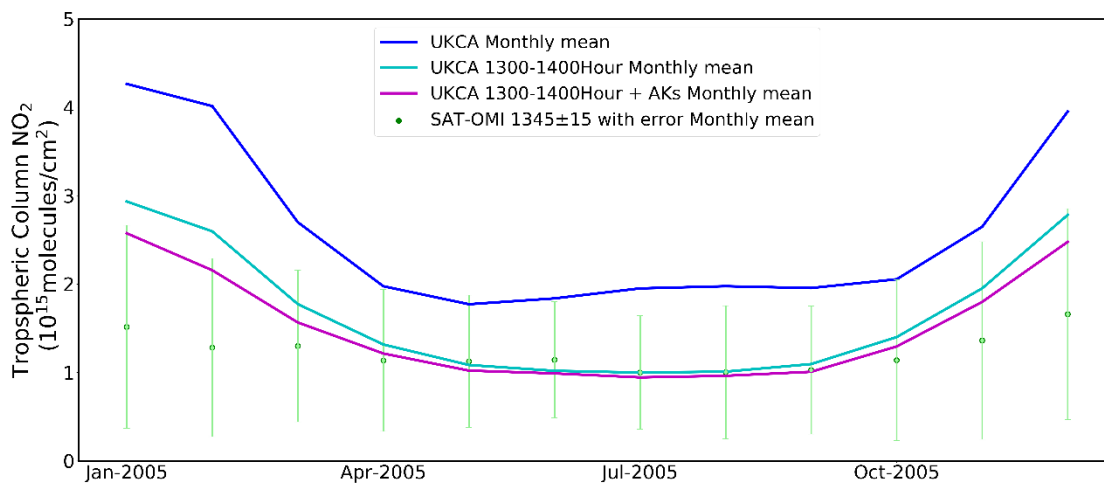


Figure 3 Average seasonal vertical profiles (2005-2015) of NO₂ (ppbv) in UKCA over (a) North India and (b) East China.

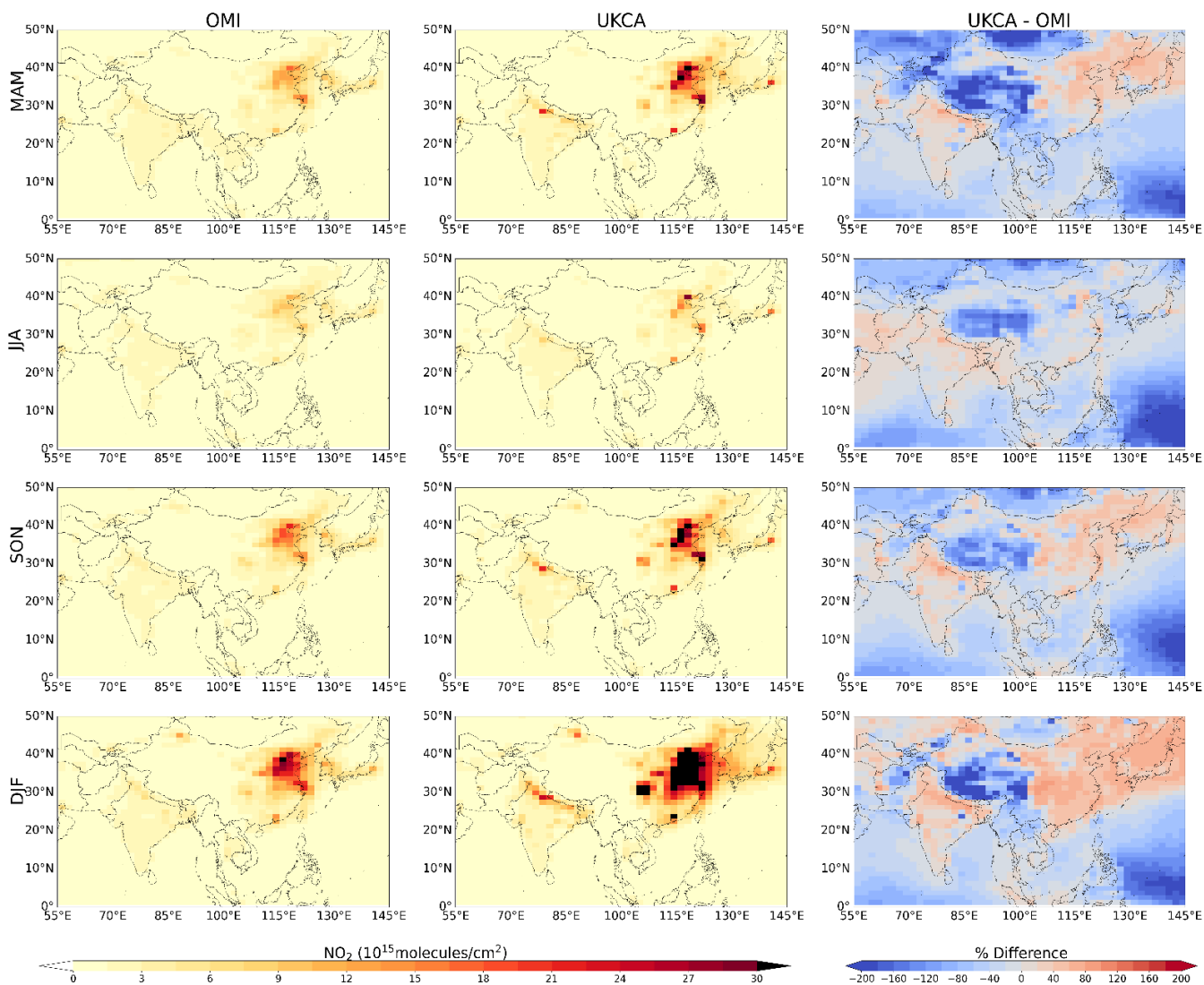
500



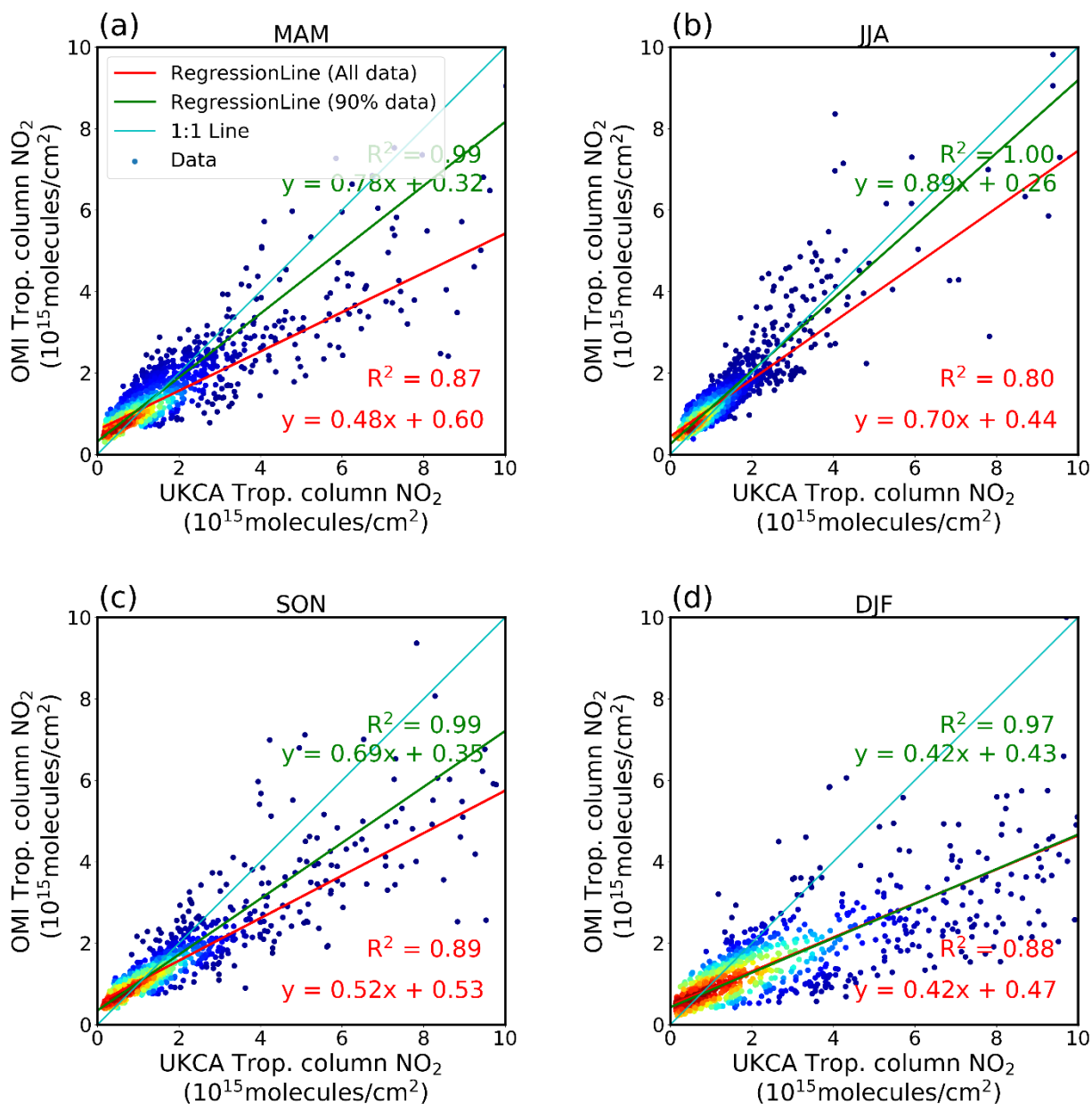
505 **Figure 4** Diurnal vertical profile of NO₂ (ppbv) simulated by UKCA over N India (left) and E China (right) for the four seasons (averaged over 2005-2015). The time axis shows the time in UTC and, in brackets, the local time. The box is the OMI overpass time. The solid black line shows the boundary layer height in the UKCA model.



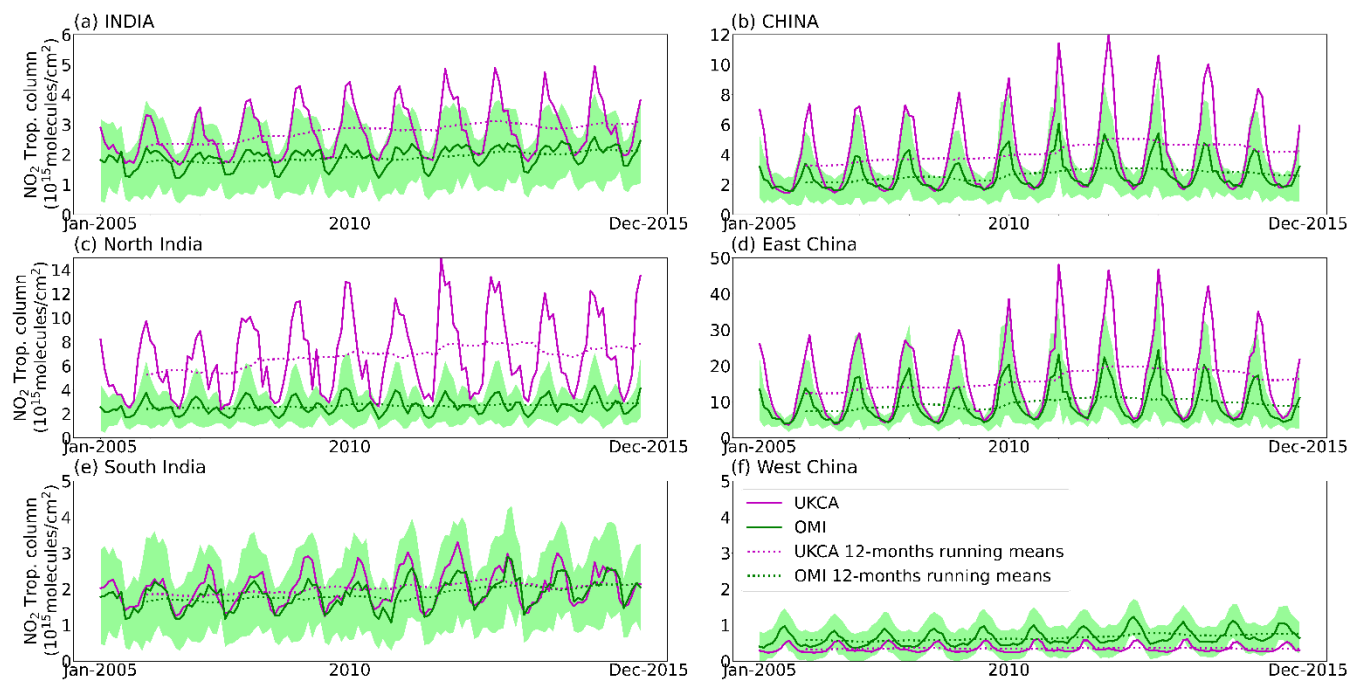
510 **Figure 5 Comparison of monthly mean tropospheric column NO₂ for 2005, averaged over the whole S/E Asia region (Figure 1) from OMI (green, with uncertainty indicated by shading), and from UKCA sampled in three different ways: (i) simple monthly mean (blue); (ii) sampled at the OMI overpass time (cyan); and (iii) sampled at the overpass time and with satellite averaging kernels applied (magenta).**



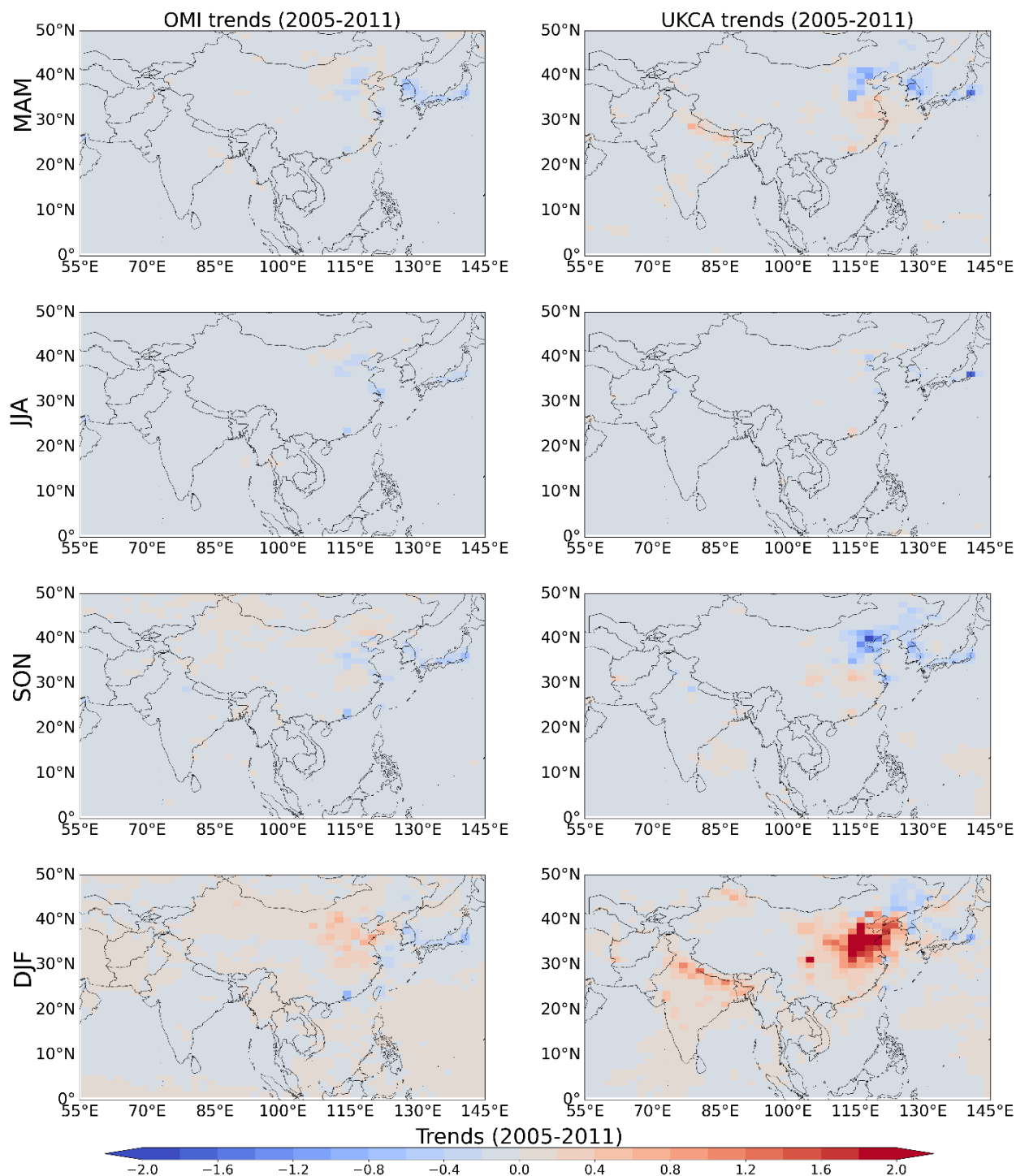
515 **Figure 6** Seasonal tropospheric column NO_2 (10^{15} molecules/ cm^2) distributions from OMI (left), simulated by UKCA (middle), and the percentage difference ($100\% \times (\text{UKCA}-\text{OMI})/\text{UKCA}$) between UKCA and OMI (right).



520 **Figure 7** Scatter plots of OMI and UKCA Tropospheric column NO₂ for the four seasons averaged over 2005-2015. Scatter data points are plotted as a heat map where red corresponds to more data. The 1:1 line is shown in cyan colour, best fit in red line (all data) and green line (lowest 90% of data). The equations of best fit and the coefficients of determination (R²) are also shown in the respective colours.



525 **Figure 8** OMI and UKCA tropospheric column NO₂ (10¹⁵ molecules/cm²) time series over (a) India, (b) China, (c) North India, (d) East China, (e) South India and (f) West China. Twelve month running means are shown in the dotted lines. Regions are indicated by the boxes in Figure 1b. Green shading represents the spread in the OMI data.



530 **Figure 9** Trends of tropospheric column NO₂ (10¹⁵ molecules/cm²/yr) from 2005 to 2011 from OMI (left) and UKCA (right) for the four seasons. Scatter plots of these data are shown in Figure 11.

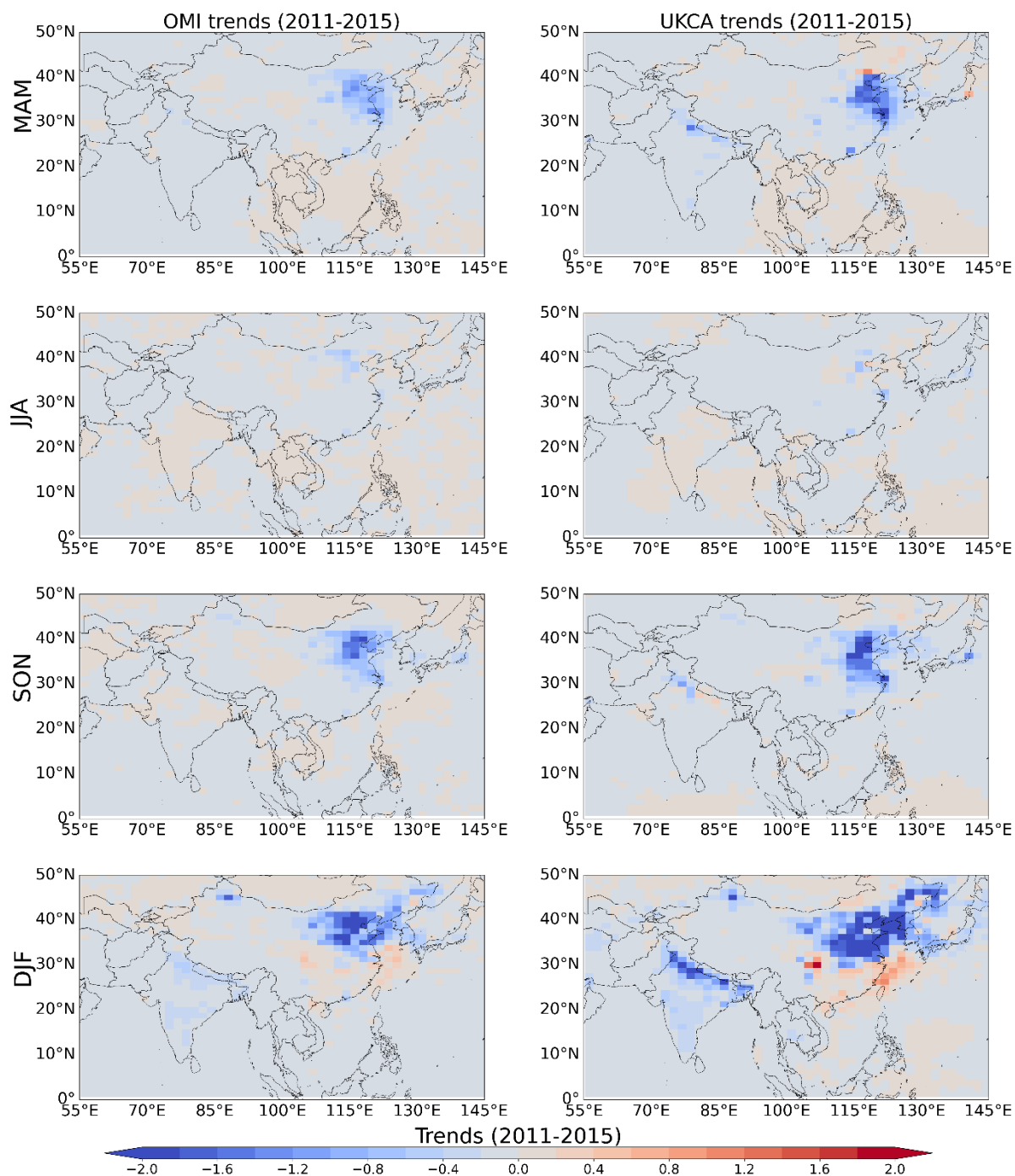
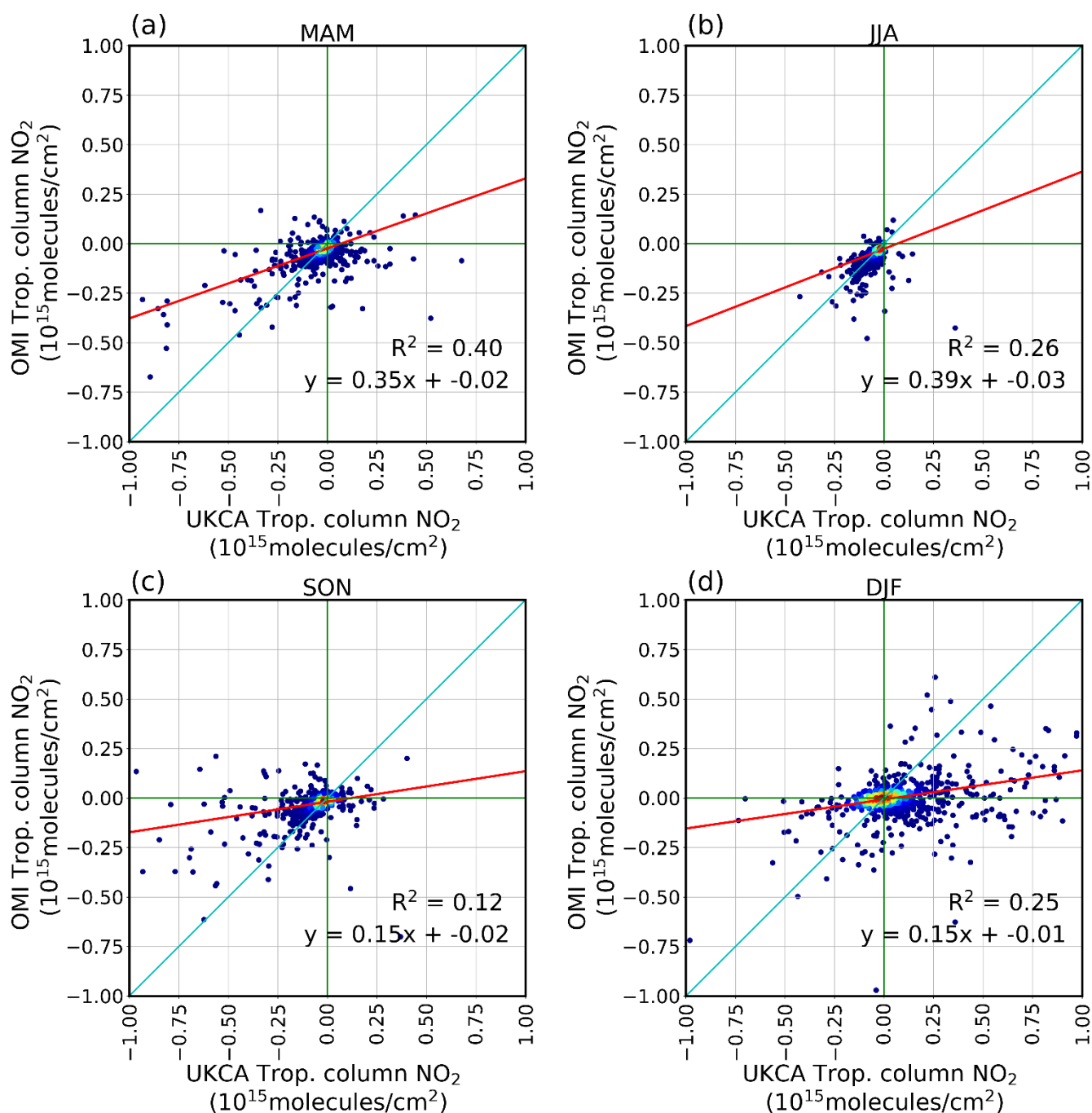


Figure 10 Trends of tropospheric column NO₂ (10¹⁵ molecules/cm²/yr) from 2011 to 2015 from OMI (left) and UKCA (right) for the four seasons. Scatter plots of these data are shown in Figure 12.



535

Figure 11 Scatter plot of UKCA and OMI tropospheric column NO₂ trends (10¹⁵ molecules/cm²/yr) from 2005 to 2011 by season. The 1:1 line is shown in cyan colour, best fit line in red colour. Data points shown as a heat map where red corresponds to more data. The equation of best fit and the coefficient of determination (R²) are also shown.



540

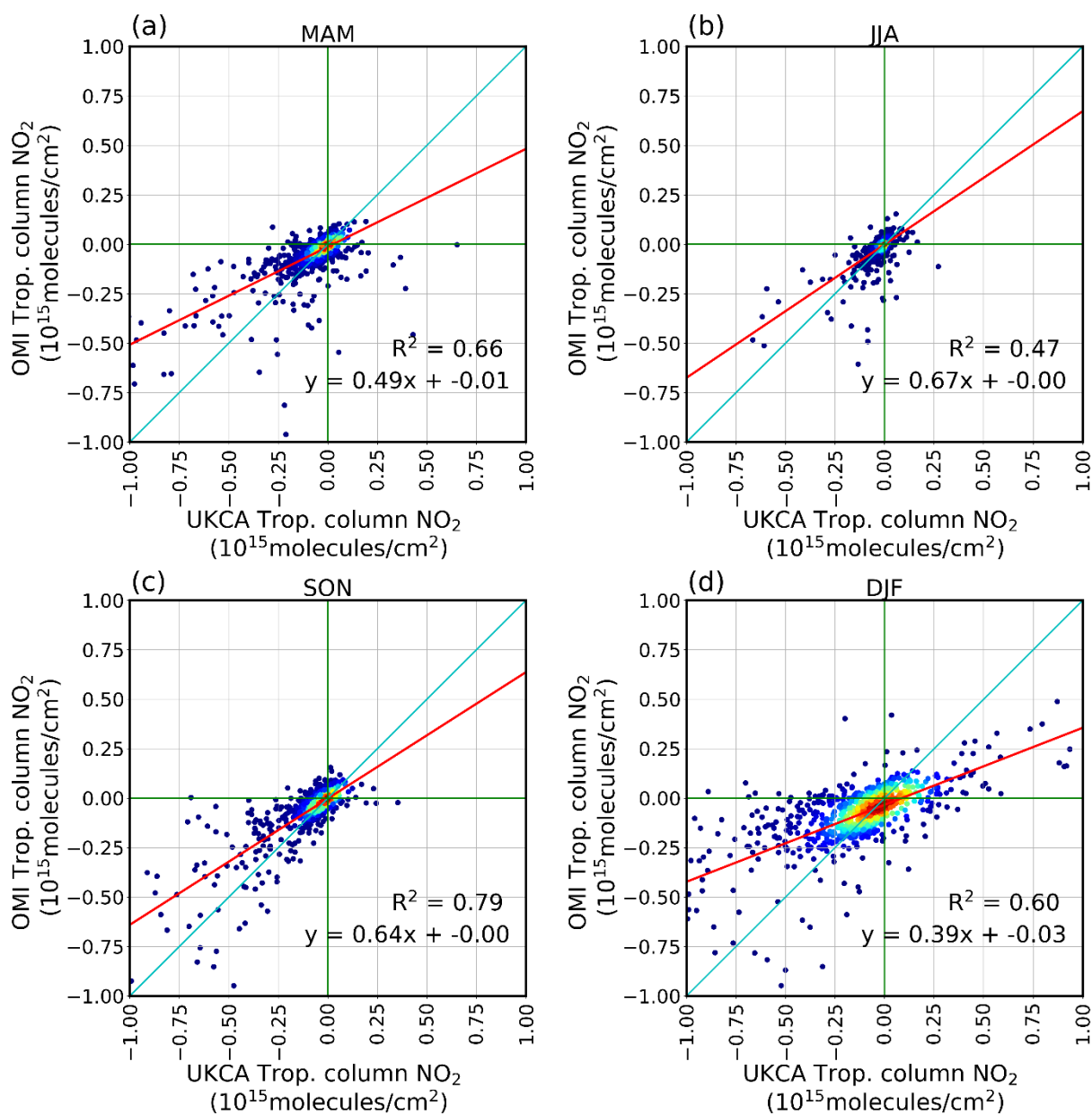


Figure 12 Scatter plots of UKCA and OMI tropospheric column NO₂ trends (10¹⁵ molecules/cm²/yr) from 2011 to 2015 by season. The 1:1 line is shown in cyan colour, best fit line in red colour. Data points shown as a heat map where red corresponds to more data. The equation of best fit and the coefficient of determination (R²) are also shown.